



Artificial pinning arrays investigated by scanning Hall probe microscopy

S.J. Bending^{a,*}, G.D. Howells^a, A.N. Grigorenko^a, M.J. Van Bael^b, J. Bekaert^b,
K. Temst^b, L. Van Look^b, V.V. Moshchalkov^b, Y. Bruynseraede^b, G. Borghs^c,
R.G. Humphreys^d

^a Department of Physics, University of Bath, Claverton Down, Bath, Som. BA2 7AY, UK

^b Laboratorium voor Vaste-Stoffysica en Magnetisme, Katholieke Universiteit Leuven, Celestijnenlaan 200D, B-3001 Leuven, Belgium

^c IMEC vzw, Kapeldreef 75, B-3001 Leuven, Belgium

^d DERA Electronics Division, St. Andrew's Road, Malvern, Worcs. WR14 3PS, UK

Abstract

High resolution scanning Hall probe microscopy has been used to study flux line pinning in a thin superconducting Pb film evaporated on top of an ordered array of ferromagnetic Co dots. After magnetisation along the easy axis, all the nanomagnets are seen to be in single domain magnetic states with dipole stray field distributions ($T > T_c$). Upon cooling through the critical temperature of the superconducting film at $H = 0$, we observe strong screening of the dipole fields which we attribute to fluxoid quantisation. After field cooling, we find that flux lines are selectively pinned at poles with the opposite sign of field and ordered structures which are commensurate with the underlying pinning array are observed. Each pinning site appears to be capable of trapping at least two flux lines, and no evidence has yet been seen for interstitial vortices at low temperatures. Results will be compared with those from the disordered pinning system found naturally in Cu-rich epitaxial YBCO thin films. These typically contain micron-sized normal Cu-rich precipitates, which have a similar density to other artificially patterned systems. We show that the precipitates act as strong pinning sites close to T_c , and also give rise to weak magnetisation peaks at average matching fields. © 2000 Elsevier Science B.V. All rights reserved.

PACS: – 74.60. – w; 74.60.Ge; 74.72.Lw; 74.80. – g

Keywords: Scanning Hall probe microscopy; Pinning arrays

1. Introduction

Recent advances in nanofabrication and thin film deposition have made it possible to produce high quality superconducting samples containing ordered pinning arrays [1–3]. The bulk magnetisation (M) and critical current (j_c) can be strongly enhanced in such samples and they have also proved to be useful

model systems for studying the microscopic nature of pinning. The commensurability effects between the periodic vortex lattice and the ordered pinning arrays have been explored and stable vortex configurations inferred from macroscopic measurements (e.g., M , j_c) or by direct imaging, e.g., Lorentz microscopy [4]. More recently, attention has turned to arrays of ferromagnetic dots where, besides the core pinning, additional contributions arise due to the interaction of the flux lines with the local magnetic

* Corresponding author.

fields of the dots [5–8]. While macroscopic commensurability effects have been observed in such systems, insight into the microscopic nature of these flux structures is still lacking. We report the use of a high resolution scanning Hall probe microscope (SHPM) to image these commensurate flux structures in a superconducting Pb film deposited over a square array of Co dots with in-plane magnetisation. Our experiments show that fluxoid quantisation at each pole of the dot causes pronounced screening of the dipole fields when the sample is zero field cooled. Upon field cooling, flux lines are preferentially pinned at the side of the dot where the stray field is opposite to that of the flux line and at high fields a range of commensurate multi-quanta vortex lattices can be distinguished.

We also present results on a ‘natural’ antidot pinning system found in Cu-rich epitaxial $\text{YBa}_2\text{Cu}_3\text{O}_{7-\delta}$ thin films containing micron-sized normal precipitates. We show that these precipitates represent strong pinning sites for flux lines, and such samples display weak commensurability effects reminiscent of ordered arrays.

2. The scanning Hall probe microscope

The SHPM used is a modified commercial low temperature STM where the tunnelling tip has been replaced by a GaAs/AlGaAs heterostructure chip. A Hall probe was defined in a two-dimensional electron gas at the intersection of two ~ 200 nm wide wires ~ 5 μm from the corner of a deep mesa etch. The latter had been coated with a thin Au layer to act as an integrated STM tip, allowing the simultaneous measurement of local magnetic induction and surface topography. In practice, the sample is first approached towards the sensor using an inertial coarse approach mechanism until tunnelling is established and then retracted ~ 100 nm allowing rapid scanning with little risk of damaging the Hall sensor. The Hall probe is mounted at an angle of $1\text{--}2^\circ$ with respect to the sample plane to ensure that the STM tip is always the closest point to the surface. We estimate that the active Hall sensor was $\sim 200\text{--}300$ nm above the sample during the scans shown here. A more detailed description of the SHPM can be found elsewhere [9].

3. Imaging in Pb films containing Co dots

Square lattices (1.5 μm period) of rectangular sub-micron magnetic dots, consisting of a trilayer of Au (7.5 nm)/Co (20 nm)/Au (7.5 nm) on an SiO_2 substrate, were fabricated by molecular beam deposition and electron-beam lithography. The dots have lateral dimensions of 540 nm (easy axis) \times 360 nm. The MFM measurements at room temperature reveal a multidomain structure in the as-grown state. After magnetisation along the easy axis, all dots are in a stable remanent single domain state. The lattice of Co dots was covered with a 50-nm superconducting Pb film, a protective Ge layer (20 nm) and a 10 nm Au layer for the STM control of the microscope. Further details of the sample fabrication and characterization are presented elsewhere [7].

Prior to the measurements, the sample was magnetised along the easy axis of the dots in a 0.5 T in-plane field. Experiments were then performed both above and below $T_c (= 7.16$ K) of the Pb film with a small magnetic field (< 20 Oe) applied perpendicular to the sample plane. The first matching field B_1 is defined as the field at which exactly one flux quantum is associated with each unit cell of the pinning array, i.e., $B_1 = \Phi_0/a^2 = 9.2$ G.

Fig. 1 shows an SHPM image of a region near the center of the sample at $H = 0$ and $T = 77$ K. At this temperature the Pb film is in the normal state and the

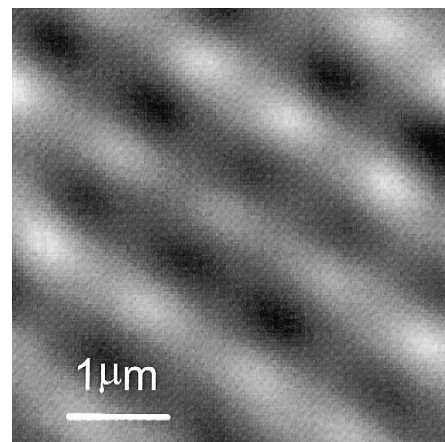


Fig. 1. SHPM image of the square lattice of single domain Co dots at 77 K. The grayscale spans ~ 4.0 G from black to white.

dipole stray fields characteristic of an ordered array of single domain particles can be clearly seen.

As the sample is zero-field cooled through T_c of the Pb film, we see a sudden increase in the amplitude of the dipole stray fields. Fig. 2 shows a plot of the measured peak-to-valley magnetic induction of SHPM images of the type shown in Fig. 1 at various temperatures. An increase of ~ 0.35 G is clearly observed below T_c , which persists down to lower temperatures. Noting that the low temperature penetration depth in the Pb film is somewhat smaller than the length of the Co dot, we attribute this observation to the need to satisfy fluxoid quantisation above each magnetic pole in the superconducting state. For $T > T_c$, such considerations do not apply and we estimate that slightly less than $1\Phi_0$ threads the film at each pole. Once the sample becomes superconducting, the flux threading the Pb film at each pole must be quantised, and screening currents flow which increase the associated flux to $1\Phi_0$.

Fig. 3 shows images of the same sample region after field cooling in $B/B_1 = -1/2$. In order to identify the vortex locations, we subtract the dipole contribution (at $T > T_c$) from the images at $T < T_c$. This is illustrated in Fig. 3a–c where the image at 7.5 K (Fig. 3b) is subtracted from that at 6 K (Fig. 3a) to generate the ‘‘difference image’’ shown in Fig. 3c containing predominantly only information

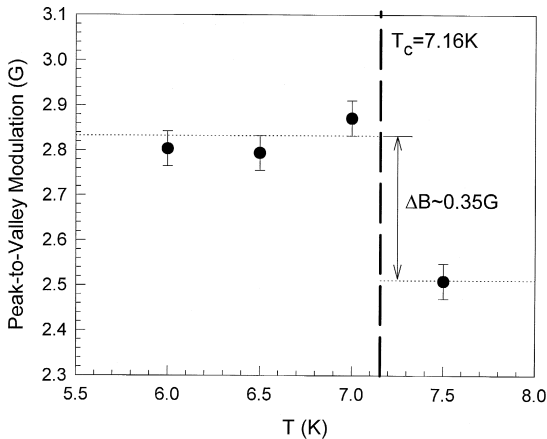


Fig. 2. Average peak-to-valley magnetic induction span over a $3 \times 3 \mu\text{m}$ area of the sample during zero field cooling. The critical temperature of the film is indicated by the vertical dashed line.

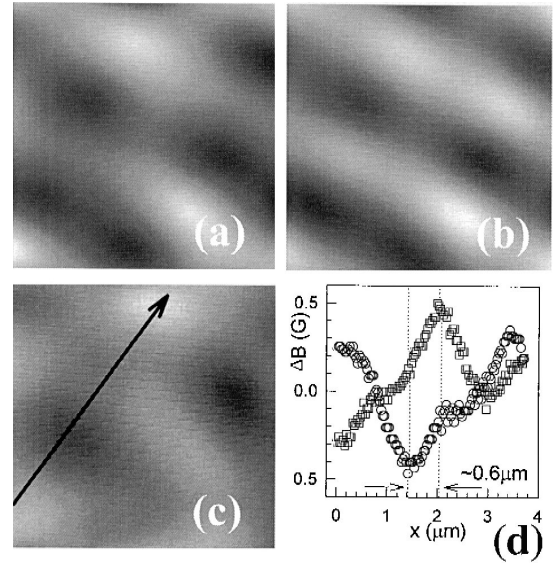


Fig. 3. SHPM images (a) at $T = 6 \text{ K} < T_c$ and $B/B_1 = -1/2$; (b) image of the same sample area at $T > T_c$ and $B/B_1 = -1/2$; (c) image obtained after subtracting (b) from (a). (d) Linescan across the difference image in the direction of arrow shown in (c) after field cooling in $B/B_1 = -1/2$ (circles) and $B/B_1 = +1/2$ (squares).

about the flux lines. Two black ‘down’ vortices are resolved in the subtracted image which are located at the white ‘up’ poles of the Co dots ($T > T_c$). This pole selectivity is not surprising since we know that a free vortex and the ‘antivortex’ represented by the opposite pole of the magnet will attract and ultimately annihilate one another. Fig. 3d shows linescans along the easy axis of the Co dots for $B/B_1 = -1/2$ and $B/B_1 = +1/2$. Upon field reversal, vortices are added in different positions and the centers of the up ($B > 0$) and down ($B < 0$) flux lines are separated by about 600 nm, which is very close to the dot length and indicates that they are selectively pinned at the opposite ends of the nanomagnets. Contrary to the case of perpendicularly magnetized dots [6] where positive ‘up’ vortices are pinned at dots with moment pointing up, the direct interaction between the (perpendicular) local vortex field and the magnetic moment of the dot can be disregarded for dots with in-plane magnetisation.

Fig. 4 shows the difference images generated as described earlier after field cooling at $B/B_1 = 1/2$,

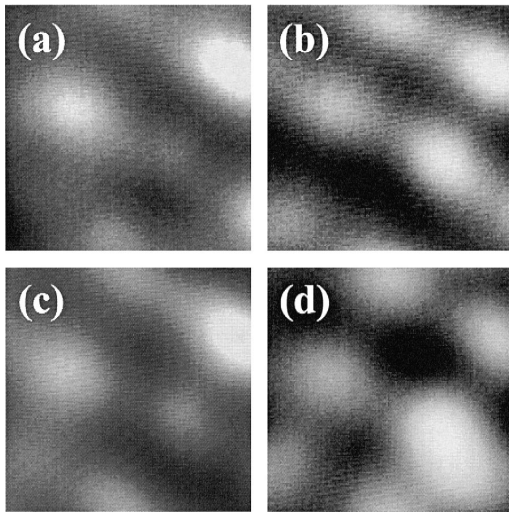


Fig. 4. SHPM images at $T = 6$ K after subtraction of the dipole field contribution at $B =$ (a) $+ B_1/2$, (b) $+ B_1$, (c) $+ 3B_1/2$, and (d) $+ 2B_1$.

1, $3/2$, and 2. In all cases, we see ordered vortex structures which are commensurate with the underlying square pinning array. At $B/B_1 = 1/2$ (Fig. 4a), we observe the ‘checkerboard’ structure where every second pinning site is occupied by a flux line forming a square vortex lattice rotated by 45° with respect to the pinning array. At B_1 (Fig. 4b), every pinning site traps a single flux line and the vortex structure mirrors that of the dot array. For $B/B_1 = 3/2$ (Fig. 4c), the structure is a direct superposition of that for $B/B_1 = 1/2$ and $B/B_1 = 1$, where half of the sites pin two flux quanta while the rest trap just one. Finally, for $B/B_1 = 2$ (Fig. 4d), every dot has trapped two flux lines, except for one dot in the bottom right corner which has three flux quanta associated with it, possibly due to a small sample inhomogeneity or because the applied field slightly exceeds $2B_1$. While the location of the first pinned vortex can be well established, it is not clear from an experimental or theoretical point of view where the second (or additional) vortices are attached. We are therefore unable to decide at this point whether we observe multi-quanta vortices with a single normal core or strongly overlapping multiple single quantum vortices. Up to $2B_1$, we see no evidence for vortices occupying interstitial positions at these low temperatures ($T < 6.5$ K). Earlier macroscopic $M(B)$ and $j_c(B)$ data on

similar samples at temperatures very close to T_c have shown an abrupt drop at $B = B_1$, which was attributed to the presence of weakly pinned interstitial vortices [1,10,11]. We note that care must be taken when comparing measurements at different temperatures, since the penetration depth will become very large close to T_c . If $\lambda(T)$ becomes larger than half the length of the Co dot, then the two magnetic poles can no longer be considered independently, and the physics of the situation is qualitatively different.

4. Imaging in YBCO films containing normal precipitates

The $\text{YBa}_2\text{Cu}_3\text{O}_{7-\delta}$ film was grown on an MgO substrate at 690°C by electron beam co-evaporation of the metals in the presence of atomic oxygen with a subsequent anneal, also in atomic oxygen [12]. The sample was grown with excess Cu to produce a random array of Cu-rich precipitates. The film used here was $0.35 \mu\text{m}$ thick, had a critical temperature of 86.4 K as measured by magnetisation, and the growth direction was (001). The precipitates consisted of a non-superconducting phase, had sizes in the range of 0.2 – $2 \mu\text{m}$ and were homogeneously distributed in the film with a density (n) of about $2 \times 10^7 \text{ cm}^{-2}$ yielding a mean matching field ($n\Phi_0$) of ~ 5 G. Fig. 5 shows a typical optical micrograph of the surface of the film containing precipitates. In contrast to the earlier work on the Pb/Co system, a lower resolution Hall probe (active area $\sim 0.8 \times 0.8 \mu\text{m}$) was used to study the YBCO film.

Unfortunately, due to poor quality tunnelling with our integrated STM tip, we were unable to simultaneously image a precipitate and a flux line pinned on it. However, the following observations reveal precipitates to be pinning centres for flux lines. For a range of field-cooled measurements with different field polarities and strengths, we find flux lines tend to be located at the same positions in the scanning area of the sample. This is illustrated for four different applied fields in Fig. 6a–d. Flux lines A, B, C, and a cluster of lines D are common to at least two of the images indicating the location of a few particularly strong pinning sites. Note that we would

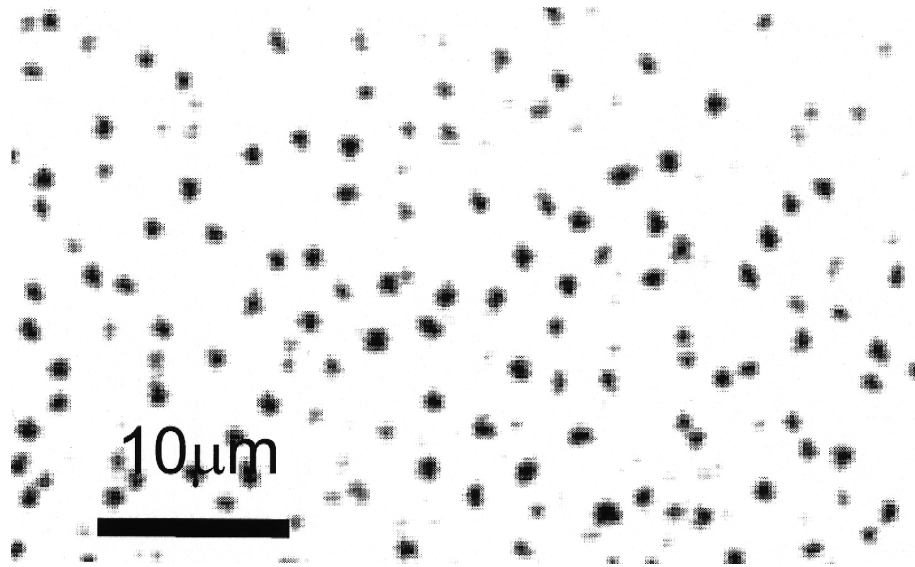


Fig. 5. Optical micrograph of a YBCO thin film with precipitates.

expect the strongest pinning precipitates to be occupied at very low fields, but this is no longer necessarily the case at higher fields due to flux line interactions.

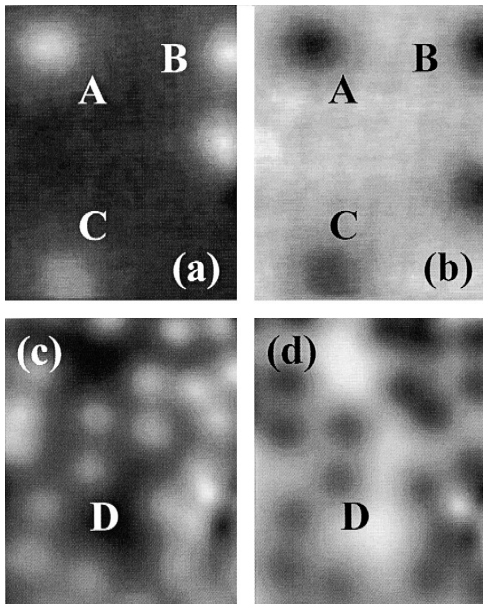


Fig. 6. SHPM images of a YBCO thin film with precipitates after field-cooling to 77 K in (a) 0.1 Oe (grayscale spans 0.73 G), (b) -0.1 Oe (0.8 G), (c) 1.1 Oe (1.1 G), (d) -0.9 Oe (1.1 G). The symbols A–D highlight common features in the images.

We also find a wide distribution of measured flux line diameters suggesting that they are pinned on precipitates of different size. This is illustrated for two neighbouring flux lines in Fig. 7a,b. Linescans in the directions indicated clearly reveal flux line A (diameter $\sim 5 \mu\text{m}$ at 77 K) to be considerably broader than flux line B (diameter $\sim 3 \mu\text{m}$ at 77 K) at all temperatures; a discrepancy that far exceeds any possible asymmetry due to the relative tilt angle between the sample and the scanning plane. Moreover, as the temperature decreases the measured flux line half-width saturates to a size which is many times larger than the dimensions of the Hall probe ($\sim 0.8 \mu\text{m}$) or a typical vortex diameter for precipitate-free YBCO films ($\sim 2 \mu\text{m}$ [13]), indicating the presence of a large core. Despite having different core sizes, the flux lines appear to have a universal decay length at a given temperature, supporting the picture of vortices pinned on precipitates. In some images we also observe two flux lines very close together ($d < \lambda$). At such small separations, flux line repulsion must be very strong indicating that both are firmly pinned on adjacent precipitates.

Finally, we have studied local magnetisation M_{loc} (as defined by $M_{\text{loc}} = B_{\text{loc}} - H_a$, where H_a is the applied field and B_{loc} is the local induction) loops for the YBCO film with precipitates at various temperatures. A typical scanning region of $25 \times 25 \mu\text{m}$

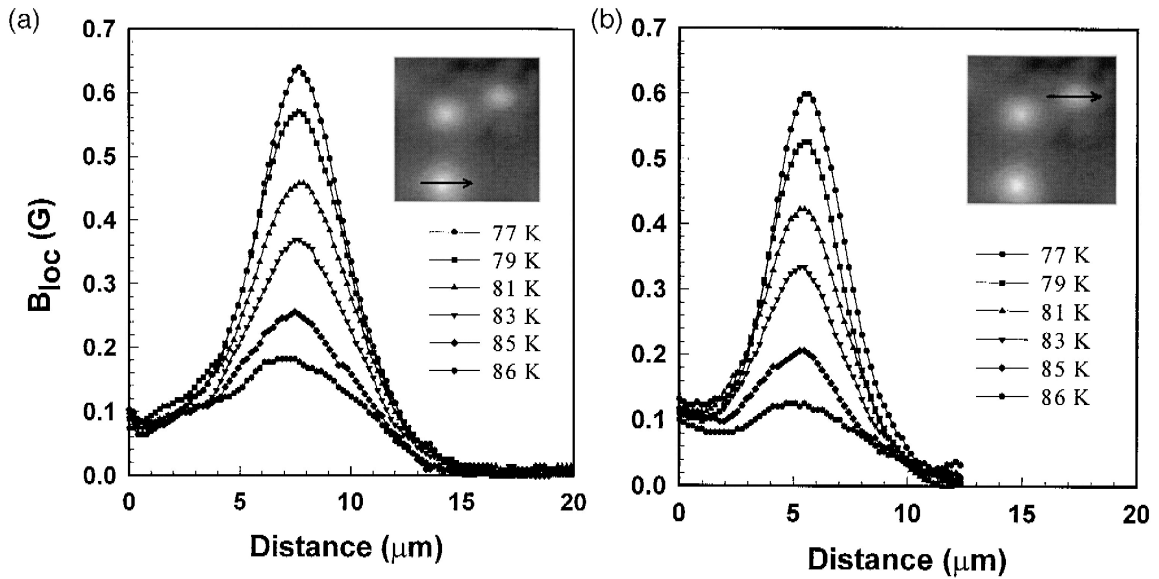


Fig. 7. Linescans across a flux line (a) at the bottom, and (b) at the top, of the SHPM image shown in the insets for a YBCO thin film with precipitates at various temperatures.

was very much smaller than the sample size yet still contained a large number (> 150) of precipitates. Thus, the average of the local magnetisation over the scan area yields the mean local response of a reason-

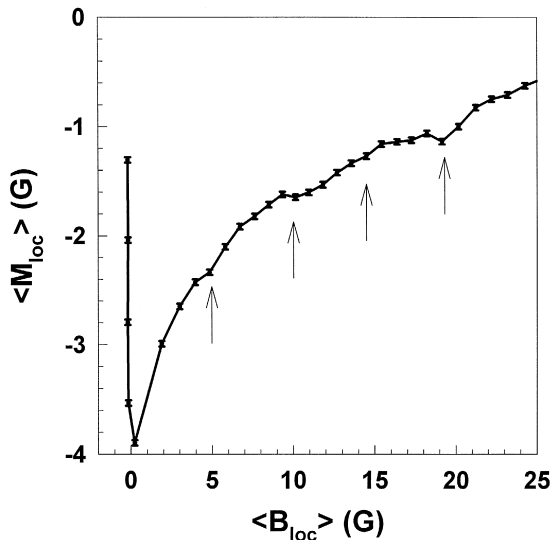


Fig. 8. The local magnetisation averaged over the scanning area as a function of the mean local induction at 86 K extracted from the initial part of the hysteresis loop after zero field-cooling.

ably large ensemble of precipitates. Fig. 8 shows the local magnetisation averaged over the scan area as a function of the mean local induction at 86 K for the initial part of a hysteresis loop after zero field-cooling. Four weak matching anomalies (plateaus and minima) can be seen at approximately equal intervals of $B_m \sim 5$ G, which are significantly larger than the noise level indicated by the error bars. These features were more pronounced for temperatures closer to the transition temperature and disappeared below 83 K. The spacing of these matching peaks is very close to the matching field estimated from optical micrographs of our films, and we conclude that their origin must be similar to that of the commensurability features observed in ordered pinning arrays.

5. Conclusions

In conclusion, we have used a high resolution SHPM to identify stable vortex configurations in thin Pb films containing square arrays of ferromagnetic pinning sites. Strong screening of the Co dipole fields is observed when the film is cooled below T_c

in zero applied field, which we attribute to fluxoid quantisation. In applied perpendicular magnetic fields, we clearly observe that the first flux line is selectively pinned at the pole of the magnet with the opposite sign of field. Ordered vortex structures, which are commensurate with the underlying pinning array, are imaged at fields up to twice the matching field.

We have also shown that the precipitates formed naturally in Cu-rich YBCO films effectively pin flux lines. Weak matching anomalies were observed in the average local magnetisation for the random array of precipitates under magnetic field sweeps. Up to four orders of matching peaks were seen in the initial part of zero field-cooled hysteresis loops as a function of the mean local induction very close to T_c .

Acknowledgements

This work was supported in the UK by EPSRC and MOD Grants No. GR/J03077 and GR/L96448 as well as the University of Bath Initiative Fund and in Belgium by the Fund for Scientific Research — Flanders (FWO), the Belgian IUAP and the Flemish GOA programs.

References

- [1] M. Baert, V.V. Metlushko, R. Jonckheere, V.V. Moshchalkov, Y. Bruynseraede, *Phys. Rev. Lett.* 74 (1995) 3269.
- [2] V.V. Moshchalkov, M. Baert, V.V. Metlushko, E. Rosseel, M.J. Van Bael, K. Temst, R. Jonckheere, Y. Bruynseraede, *Phys. Rev. B* 54 (1996) 7385.
- [3] V.V. Moshchalkov, M. Baert, V.V. Metlushko, E. Rosseel, M.J. Van Bael, K. Temst, R. Jonckheere, Y. Bruynseraede, *Phys. Rev. B* 57 (1998) 3615.
- [4] K. Harada, O. Kamimura, H. Kasai, T. Matsuda, A. Tonomura, V.V. Moshchalkov, *Science* 274 (1996) 1167.
- [5] J.I. Martin, M. Vélez, J. Nogués, I.K. Schuller, *Phys. Rev. Lett.* 79 (1997) 1929.
- [6] D.J. Morgan, J.B. Ketterson, *Phys. Rev. Lett.* 80 (1998) 3614.
- [7] M.J. VanBael, K. Temst, V.V. Moshchalkov, Y. Bruynseraede, *Phys. Rev. B* 59 (1999) 14674.
- [8] I.F. Lyuksyutov, V. Pokrovsky, *Phys. Rev. Lett.* 81 (1998) 2344.
- [9] A. Oral, S.J. Bending, M. Henini, *Appl. Phys. Lett.* 69 (1996) 1324.
- [10] E. Rosseel, M.J. Van Bael, M. Baert, R. Jonckheer, V.V. Moshchalkov, Y. Bruynersaede, *Phys. Rev. B* 53 (1996) R2983.
- [11] K.M. Beauchamp, T.F. Rosenbaum, U. Welp, G.W. Crabtree, V.M. Vinokur, *Phys. Rev. Lett.* 75 (1995) 3942.
- [12] N.G. Chew, *IEEE Trans. Appl. Supercond.* 5 (1995) 1167.
- [13] A. Oral, S.J. Bending, R.G. Humphreys, M. Henini, *Supercond. Sci. Technol.* 10 (1997) 17.